1994A&A...281..199S

Astron. Astrophys. 281, 199–208 (1994)

ASTRONOMY AND ASTROPHYSICS

The HI gas kinetic temperature of high galactic latitude cirrus clouds

Ronald Stark[1], **John M. Dickey**[2], **W.B. Burton**[1], **and Alexander Wennmacher**[3]

[1] Sterrewacht Leiden, P.O. Box 9513, NL-2300 RA Leiden, The Netherlands
[2] Department of Astronomy, University of Minnesota, 116 Church Street SE, Minneapolis, Minnesota 55455, USA
[3] Radioastronomisches Institut der Univerität Bonn, Auf dem Hügel 71, D-53121 Bonn, Germany

Received May 24, accepted August 3, 1993

Abstract. We present the results of a combined absorption and emission study of the H I 21 cm line toward several cirrus clouds at high galactic latitude. The absorption measurements were obtained with the Very Large Array (VLA) synthesis telescope, the emission data with the Effelsberg telescope. The three cirrus complexes studied were selected from the Deul & Burton (1990) study. Deul & Burton had shown that these cirrus clouds have associated H I emission with radial velocities near 0 km s^{-1} as well as with more extreme velocities of $v < -20$ km s^{-1}. Absorption against background continuum sources was detected in 40% of the lines of sight investigated. The H I line was always found to be optically thin, $\tau < 0.6$. The 0 km s^{-1} component was found in each direction where absorption was detected; in addition, three directions showed absorption at intermediate negative velocities. The derived apparent spin temperatures vary between 20 K and > 350 K. The emission profiles reveal much more widely distributed gas than is visible in absorption. Only the cool clumps in the cirrus show up in absorption. The observations suggest a collision of a high velocity cloud with the galactic disk gas, by which different parts of the cirrus are at present seen in different phases of shock completion. This model may explain the large observed differences in the H I emission and absorption profiles over small distances on the sky, as well as the variation of the far–infrared brightness ratio.

Key words: interstellar medium: atoms – clouds – kinematics and dynamics – structure – galaxy: solar neighbourhood – radio lines: interstellar

1. Introduction

Obervations made with the Infrared Astronomical Satellite (IRAS) revealed a large–scale component of filamentary emission from diffuse interstellar dust. This emission was named "cirrus" by Low et al. (1984), because of its morphological similarity to terrestrial clouds. The far–infrared (FIR) emission of cirrus is generally ascribed to dust continuum emission, although a significant contribution of atomic fine structure line emission from e.g. O I(63 μm) may be present (Harwit et al. 1986; Stark 1990). Low et al. identified an H I counterpart for several of their IR cirrus features in the 21 cm data of Heiles & Habing (1974), but were unable to demonstrate the IR/H I correlation in others. Deul & Burton (1990) subsequently obtained more sensitive H I data over a broader range in velocity and verified that each of the Low et al. cirrus has an H I counterpart. It thus appears that cirrus clouds are generally associated with substantial quantities of atomic hydrogen gas (e.g. Boulanger et al. 1985) and that this association frequently involves H I gas at anomalous velocities (Deul & Burton 1990; Burton et al. 1992).

It is important to ask which phases of atomic hydrogen are present in cirrus clouds, and how these phases are mixed. Goldsmith et al. (1969) showed that phases of warm (8000 K) and cold (80 K) gas can coexist in pressure equilibrium. A third component that has not yet been fitted into this picture is the so-called lukewarm H I gas (Kulkarni & Heiles 1987) with temperatures around 500 K (Kalberla et al. 1985). The kinetic temperature structure of gas in interstellar clouds may be determined using a combination of H I absorption studies toward background continuum sources and emission studies of H I in the vicinity. Absorption spectra show preferentially the cool gas, because the opacity of the 21 cm line is proportional to column density divided by temperature, N/T. In contrast, emission spectra of optically thin cirrus show the total column density of H I as a function of velocity independent of temperature, since for the H I line $h\nu << kT$ in all interstellar environments (e.g. van de Hulst 1957).

Another important question concerns the dynamical state of cirrus clouds. Many cirrus have a FIR morphology showing a diffuse transition to the sky background on one side but a very sharp transition on the opposite side (e.g. Gredel et al. 1992; Stark 1993). Kinematic unravelling of cirrus clouds by examining the velocity structure in H I features spatially correlated with the dust ones (Deul & Burton 1990; Burton et al. 1992) has shown that although most cirrus have LSR radial velocities

Send offprint requests to: R. Stark

© European Southern Observatory • Provided by the NASA Astrophysics Data System

1994A&A...281..199S

within a few km s^{-1} of zero, quite a few have components at anomalous velocities, extending into the regime of the intermediate velocity H I clouds, at $v < -20$ km s^{-1}. Thus both spatial and kinematic characteristics strongly point to the presence of shocks. We introduce the term "fossil shock" morphology for cirrus clouds which have only a local radial velocity component and a FIR morphology as described above. Other than the morphological and kinematic information, relatively little is known to date about the physical properties of these cirrus clouds.

We have undertaken an H I absorption and emission study for three of the cirrus clouds studied by Deul and Burton. These clouds lie at high galactic latitude where there is relatively little contamination with unrelated H I structures along the line of sight. The absorption spectra taken with the Very Large Array (VLA) preferentially reveal the cool gas. The emission, dominated by warmer gas, was measured with the Effelsberg 100 m telescope. In this paper we compare the emission and absorption measurements to determine the kinetic temperature of the cold/warm H I gas mixture in cirrus. We also investigate whether the anomalous velocities of some clouds may have been caused by an interaction with the galactic disk gas.

2. Observations and data reduction

We chose candidate fields after searching for background continuum sources in the Condon & Broderick (1985, 1986) survey whose positions place them near emission maxima in the IRAS FIR maps of Deul & Burton (1990). Then snapshot continuum observations were taken at 1.4 GHz in 25 VLA primary beam areas (HPBW= 32 arcmin) to see which sources are resolved and compact, and give a strong VLA flux. From that search, eleven fields were selected for the spectral line observations and observed with the VLA in its B configuration in the spring of 1989. We list the positions and peak fluxes of all continuum sources more intense than 10 mJy in Table 1. The H I observations were made by splitting the autocorrelator in 2×128 channels, spaced by 6.10 kHz (1.29 km s^{-1}), in order to observe both senses of circular polarization simultaneously with a total bandwith of 781 kHz (165 km s^{-1}). The centre frequency was set to correspond to $v = -25$ km s^{-1} with respect to the LSR. Standard sources for calibration were observed every hour. To avoid contamination with H I absorption, we used a velocity offset of 300 km s^{-1} for the observations of the bandpass calibrators.

The data were reduced using the Astronomical Image Processing System (AIPS) on a Sun workstation at the University of Minnesota. We first reduced and calibrated the gains and phases of the continuum observations. After that, we made maps of the continua and determined the peak fluxes. Next, we determined the frequency response of the antenna gains. We have removed six antennas to get a smooth bandpass. The noise in the bandpass is 20 mJy. In order to get a flat bandpass we have thrown away 17 and 20 channels at the left and right edges, respectively, where the bandpass response drops below 80%. After interpolation of the antenna gains and bandpass calibration over all sources of the line data, we extracted the individual sources from the data file and made data cubes of each subfield. The optical depth spectra were calculated using the method described in Dickey et al. (1992). This involved determining the continuum at frequencies away from the H I line and subtracting this continuum from each on–source pixel, and then averaging all spectra toward the background source over the area of the continuum emission which has a level above 50% of the continuum peak, weighted by the square of the continuum strength. The noise in the absorption spectra varies from source to source and is listed in Table 1.

The emission observations were carried out at the same positions as given in Table 1 with the Effelsberg 100 m radio telescope (HPBW= 9 arcmin) in the fall of 1991. The autocorrelator was split in 2×512 channels with the same bandwidth as for the absorption study. The obervations were carried out in frequency switching mode, switching over 3.5 MHz. The intensity calibration was based on observations of the standard source S7. Data reduction and correction for stray radiation using the method described by Kalberla et al. (1980, 1982) were done with the Bonner Astronomisches Bildrechner System (BABSY). The accuracy of the stray radiation correction is of the order 0.1–0.2 K. The rms-noise in the emission spectra is approximately 0.06 K. After this reduction process, the data were regridded to the same velocity resolution as the VLA observations, using Fourier interpolation. The Effelsberg emission data show no evidence of H I absorption against the background continuum sources, because of beam dilution.

The H I emission and absorption data were combined to estimate the spin temperatures using the ANALYZ spectral line package. Baselines were subtracted by fitting a polynomial of order three to line–free intervals. We then computed the $1 - e^{-\tau}$ spectrum. In case of non–detection, we calculated upper limits for the optical depth as 3 times the rms-level after Hanning smoothing. Finally, we calculated the apparent spin temperatures using the measured optical depths, or lower limits derived from the absorption spectra, together with the brightness temperatures at the corresponding velocities, using the relationship

$$T_{\rm spin} = \frac{T_B}{(1 - e^{-\tau})} + T_{\rm bg}, \qquad (1)$$

where $T_{\rm bg}$ is the 2.7 K background radiation. The details of deriving the brightness temperatures that correspond to the detected absorption lines and the limitations of the method are discussed in Sect. 4.1.

3. Results

Figure 1 shows the emission, absorption, and apparent $T_{\rm spin}$ (Sect. 4.1) spectra of our sources. The dashed lines denote the 3σ rms-levels of the absorption spectra. We give in Table 1 the positions and maximum fluxes ($S_{\rm max}$) of the continuum sources, together with the optical depths, central velocities, and full width at half maxima of the absorption spectra estimated from Gaussian fitting. We also list the brightness temperatures of the associated emission.

© European Southern Observatory • Provided by the NASA Astrophysics Data System

1994A&A...281..199S

Table 1. Observed sources and results of the absorption and emission study

Source	RA (1950) h m s	Dec (1950) ° ′ ″	l °	b °	S_{max} mJy	τ	rms K	v km s^{-1}	Δv km s^{-1}	T_B K	T_{spin} K
AF01n1	11:51:32.2	17:48:30.3	245.92	73.66	333	0.15(0.01)	0.01	−2.0(0.1)	3.5(0.3)	16	110
						<0.03				5	>235
AF01n2	11:50:31.8	17:50:05.7	245.32	73.48	12	<0.3	0.2			20	>60
										7	>20
BX02n1	12:10:59.2	13:24:01.0	268.74	73.42	1192	<0.01	0.006			3	>250
										5	>450
BX03n1	12:11:53.7	14:19:39.1	267.67	74.33	674	<0.02	0.01			2	>100
										7	>300
BX05n1	12:14:35.5	12:43:55.1	272.55	73.27	12	<0.3	0.1				>19
											>19
BX05n2	12:13:15.7	12:38:23.7	271.71	73.04	282	<0.02	0.01			6	>300
										4	>200
BX05n3	12:12:20.8	12:32:47.4	271.19	72.85	13	<0.3	0.1			4	>15
										2.5	>10
BX06n1	12:01:39.4	11:44:28.0	265.35	70.80	18	<0.2	0.1			4	>20
										2	>10
BX06n2	12:02:19.6	11:41:27.1	265.86	70.85	34	<0.1	0.06			5	>35
										1.5	>10
BX06n3	12:02:22.0	11:40:04.3	265.90	70.83	52	<0.1	0.05			4.5	>50
BX06n4	12:01:53.1	11:45:51.9	265.46	70.85	570	0.0407(0.0005)	0.006	−14.3(0.2)	2.68(0.04)	4	102
BX07n1	12:20:50.7	10:49:03.9	279.88	72.15	11	<0.6	0.30			11	>20
BX07n2	12:20:36.3	10:45:38.5	279.77	72.07	539	0.1279(0.0003)	0.01	−11.034(0.005)	2.83(0.01)	11	90
						0.055(0.002)		−0.87(0.02)	1.68(0.08)	4	85
BX07n3	12:19:36.9	10:39:15.5	279.16	71.88	19	0.57(0.02)	0.30	−1.03(0.08)	5.14	4	9
										4	>20
CH01n1	22:54.38.5	16:42:26.9	87.49	−37.90	703	0.085(0.001)	0.008	−0.894(0.02)	2.95(0.05)	15	180
						0.092(0.008)		−19.1(0.1)	2.974(0.003)	7	115
						0.052(0.003)		−14.84(0.07)	2.6(0.2)	14	135
						<0.02				7	>350
CH02n1	22:51:29.5	15:52:54.5	86.11	−38.18	12700	0.094(0.002)	0.002	−0.80(0.05)	5.9(0.01)	17	160
						0.258(0.003)		−10.21(0.01)	2.89(0.03)	12	30
						0.04(0.02)		−34(1.2)	2.02(0.04)	4	90
CH05n1	22:49:07.7	18:32:44.1	87.35	−35.65	1840	0.051(0.003)	0.003	1.4(0.3)	9.3(0.6)	19	300
CH06n1	22:47:13.6	16:58:56.8	85.81	−36.70	54	0.51(0.04)	0.04	−13.2(0.1)	2.7(0.3)	13	22
						<0.07				15	>200
										2	>25
CH06n2	22:47:07.5	16:47:59.7	85.66	−36.84	262	0.045(0.007)	0.01	−14.5(0.4)	5.1(0.9)	8	180
						0.040(0.002)		−1.1(0.1)	4.62(0.03)	14	480
						<0.02				8	>300
CH06n3	22:46:53.6	16:45:20.4	85.57	−36.84	36	<0.1	0.08			14	>100
										10	>70
										9	>60

The absorption profiles may be adequately represented by a single Gaussian; the emission profiles, on the other hand, are commonly a superposition of several velocity components of different widths, as can be seen from Fig. 1. Large variations in the emission and absorption profiles occur over distances on the sky as small as 12 arcmin. The optical depth of the H I gas associated with the dust cirrus structures is in all cases small: $\tau < 0.6$. We discuss below the results for the individual regions.

AF field

This cirrus feature was called the "angular feature" (AF) by Deul (1988) because of its FIR morphology. In Fig. 2 we show the IRAS 100 μm map of this cloud, together with the locations of the background continuum sources. Deul & Burton (1990) and Burton et al. (1992) found a spatial correlation between the FIR dust emission and the emission of the negative-velocity H I gas between $v = -40$ km s^{-1} and $v = -20$ km s^{-1}, as well as with the gas near $v = 0$ km s^{-1}; evidently the FIR cirrus comprises to kinematically quite different components.

© European Southern Observatory • Provided by the NASA Astrophysics Data System

1994A&A...281..199S

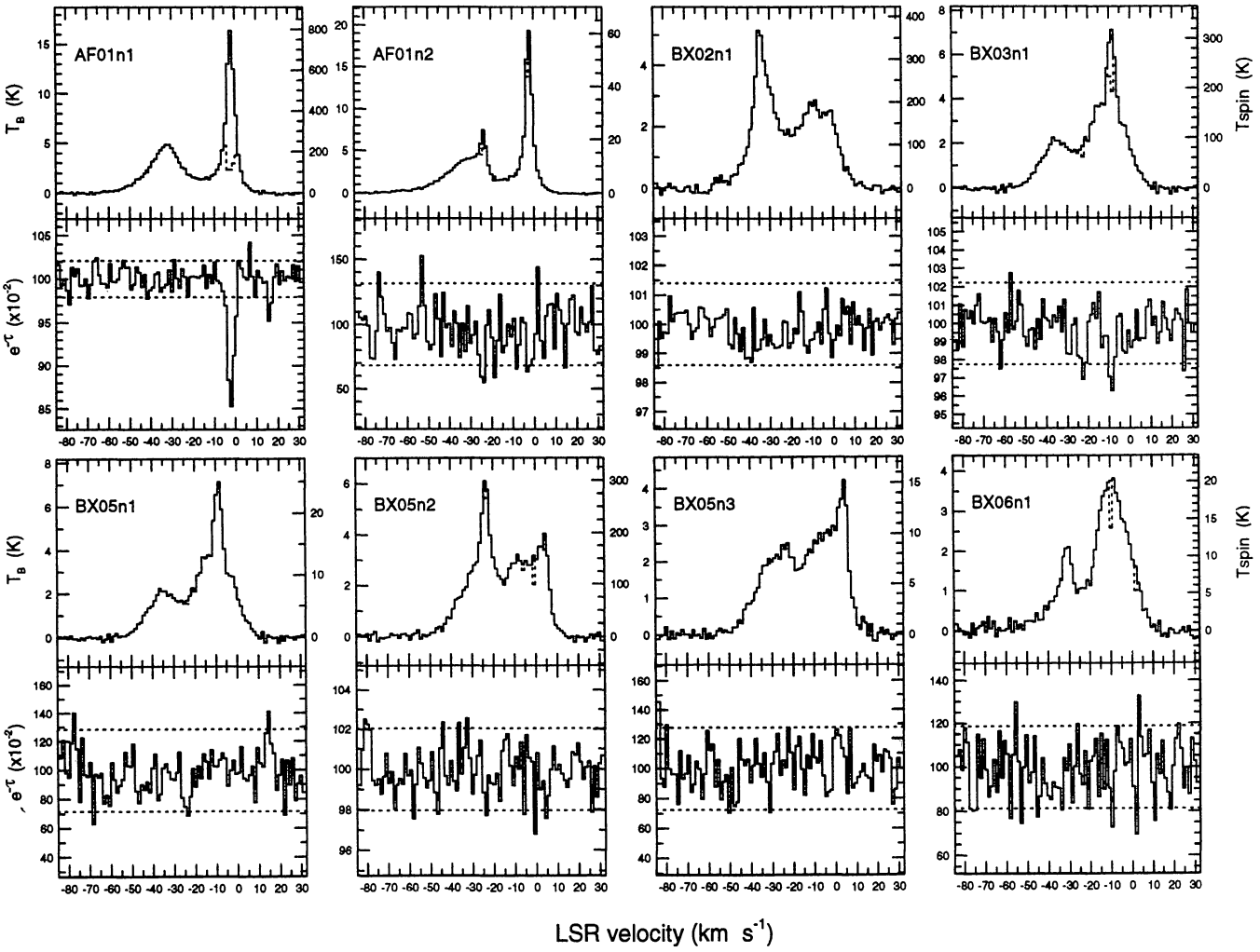

Fig. 1. Emission, absorption, and $T_{\rm spin}$ spectra of the observed sources. The dashed lines denote the $\pm 3\sigma$ rms-levels of the absorption spectra

AF01n1– We detect absorption only in the narrow velocity component at $v = -2.0$ km s^{-1}, yielding an H I temperature $T_{\rm spin}$= 110 K. The broad emission component centred near $v = -35$ km s^{-1} does not show up in absorption, leading to a lower limit $T_{\rm spin} > 235$ K.

AF01n2– This position is located 14 arcmin away from AF01n1, corresponding to 0.4 pc at a distance of 100 pc, which seems plausibly representative for high latitude cirrus (Penprase 1992). (We have no direct distance measurements of the cirrus discussed here, but adopt 100 pc throughout.) A tentative detection appears at the position of the narrow component near $v = 0$ km s^{-1}, as well as at the narrow component which is superimposed on the broad H I emission component near $v = -25$ km s^{-1}. If these are real, we derive spin temperatures for these components of 20 and 60 K, respectively.

BX field

This complex cirrus field was identified by Low et al., who gave the two principal components the names "B" (centred near $l = 275°, b = 75°$) and "X" (centred near $l = 275°, b = 72°$). Figure 3 shows the 100 μm map and the location of the background sources. Deul and Burton found that the H I emission of feature B is most intense near $v = -18$ km s^{-1}, but that it extends into the anomalous velocity regime to about $v = -40$ km s^{-1}. Feature X peaks near $v = -8$ km s^{-1}. Also for these clouds there is a tight spatial correlation between the H I emission in specific velocity intervals and the FIR emission defining the features. The spectra BX02–BX05 lie in the direction of feature B; the spectra BX06 and BX07, in the direction of feature X.

BX02n1– The H I emission shows a narrow component near $v = -35$ km s^{-1} and a broad component near $v = -10$ km s^{-1}. No absorption is detected; we derive a lower limit for the spin temperature of the narrow component $T_{\rm spin} > 450$ K. There is some indication from the emission spectrum that the broad component consists of several narrow components, for which we derive spin temperature limits $T_{\rm spin} > 200$ K.

BX03n1– This position is located 57 arcmin from BX02n1 (corresponding to 1.7 pc at a distance of 100 pc). Note the different location of the narrow component compared to BX02n1. Two tentative absorption lines are detected near $v = -10$ km

© European Southern Observatory • Provided by the NASA Astrophysics Data System

1994A&A...281..199S

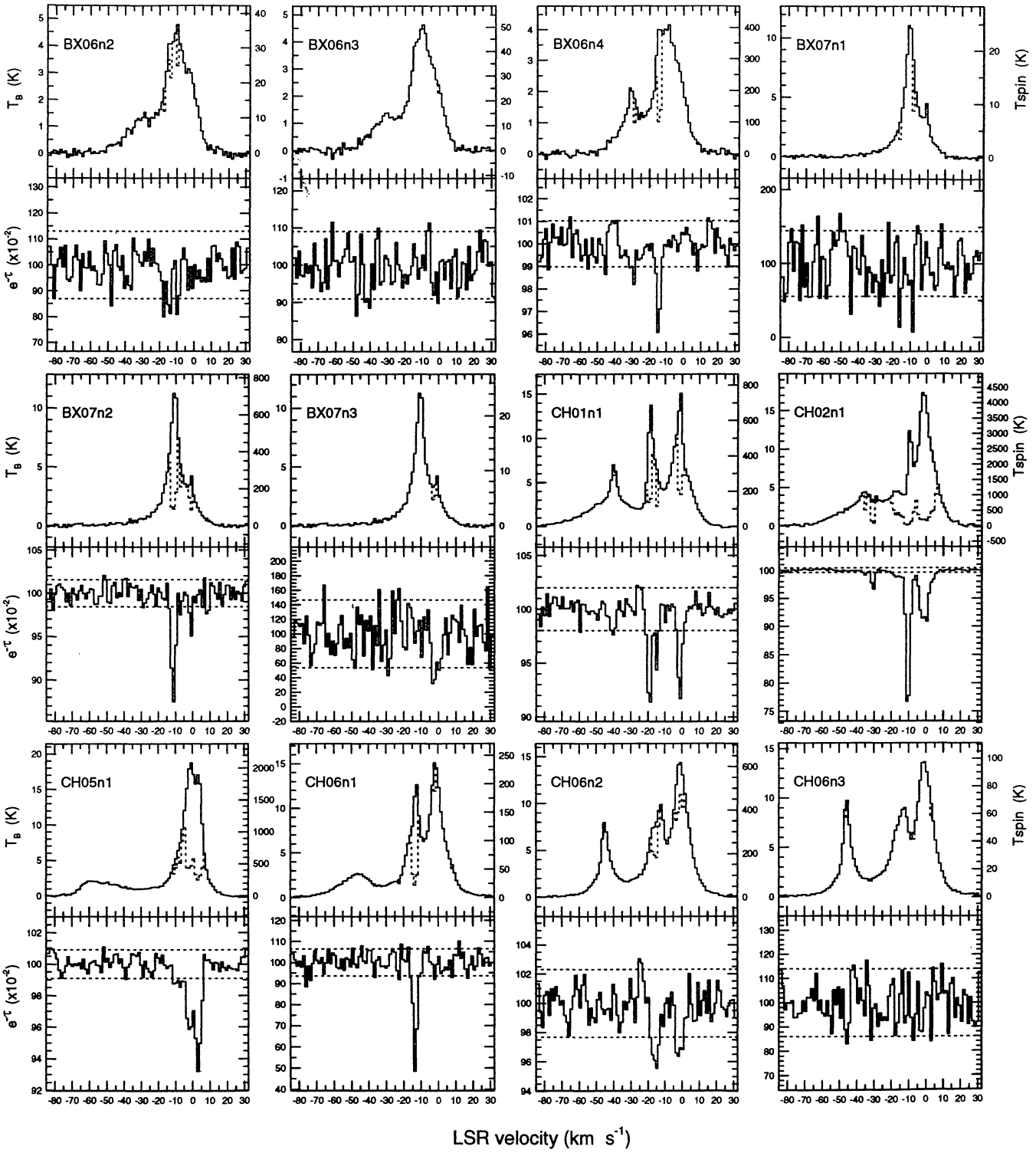

Fig. 1. (continued)

© European Southern Observatory • Provided by the NASA Astrophysics Data System

1994A&A...281..199S

s^{-1} and $v = -25$ km s^{-1}, with spin temperatures of 180 and 100 K, respectively.

BX05– The positions of n1, n2, and n3 lie 15–35 arcmin (0.9–2.4 pc) apart, 57 arcmin (1.7 pc) from BX02n1. Note the large differences between the velocities of the narrow components in the individual emission spectra of BX05n1 and BX05n2, which lie only 20 arcmin (0.6 pc) apart. No absorption is found. Because of the large rms-values we sometimes find weak lower limits for the kinetic temperature. In case of a low rms-value (n2), where the flux of the continuum is an order of magnitude larger, we find better limits. The lower limits vary between 15 and 300 K.

BX06– These sources lie close to each other at distances varying from 1.5–11 arcmin (0.04–0.3 pc). Their emission spectra are all similar in shape, except for the narrow velocity component which is present in n1 near $v = -30$ km s^{-1}. We only find absorption in the directions of n2 and n4. The spin temperatures we find are 35 K and 102 K at $v = -14.3$ km s^{-1} for n2 and n4, respectively. For the other sources we derive weak lower limits, because of the high noise in the absorption spectra.

BX07– The emission spectra show only emission near $v = -10$ km s^{-1}; the absorption spectra show several components near this velocity. The lowest spin temperature we derive is 9 K (BX07n3); the highest, 90 K (BX07n1). These two positions are only 21 arcmin (0.6 pc) apart.

CH field

This feature was called the "coathanger" (CH) by Deul (1988) because of its appearance at 100 μm. Deul & Burton (1990) found that most of the H I gas in this direction emits at velocities near $v = -5$ km s^{-1}, but also that the 100 μm emission near $l = 86°, b = -38°$, is associated with H I at quite extreme negative velocities up to $v = -51$ km s^{-1}. (We note that such velocities are outside the band of the Heiles & Habing (1974) survey.) Figure 4 shows the 100 μm emission of this feature together with the positions of the absorption measurements.

CH01n1– Three narrow components, well separated in velocity, can be recognized in emission; only two of these show up in absorption. The -20 km s^{-1} component shows two distinct absorption lines. The derived spin temperatures near $v = 0$ km s^{-1} and $v = -20$ km s^{-1} have values near 100 and 200 K, respectively, whereas the $v = -40$ km s^{-1} component has a spin temperature above 350 K.

CH02n1– The background continuum source is known as 3C454.3 (Bridle et al. 1972). This source is located at 1°.1 (2.0 pc) from CH01n1. Its absorption spectrum is taken toward the strongest background source of our sample and has therefore the highest signal–to–noise ratio. We find four absorption features: near $v = 0, -10, -30$, and -35 km s^{-1}. The derived spin temperatures are 160, 30, 90, and 100 K, respectively. This line of sight has also been studied by Dickey et al. (1978) using the Arecibo radio telescope. They derived spin temperatures of 65 and 100 K near $v = -10$ km s^{-1} and $v = -30$ km s^{-1}, respectively.

CH05n1– The absorption spectrum is 2°.3 (3.9 pc) from CH01n1 and consists of several components for which we derive spin temperatures between 200 K and 400 K. Note the broad low-level emission component near $v = -60$ km s^{-1}.

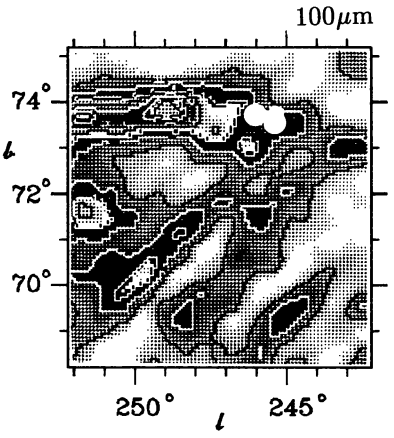

Fig. 2. IRAS 100 μm map of the cirrus cloud "AF" (adapted from Deul & Burton 1990) together with the positions of the absorption and emission measurements. The lowest contour is at 1.2 MJy $ster^{-1}$ and increases with steps of 0.35 MJy $ster^{-1}$

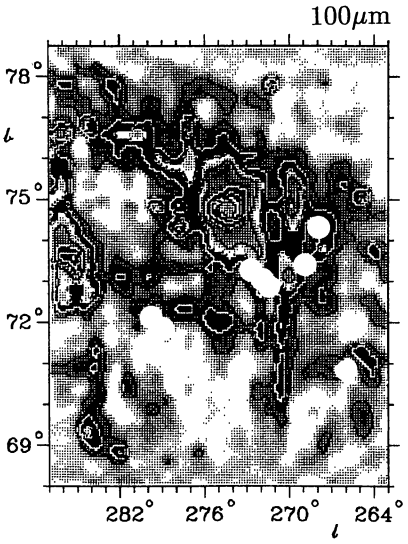

Fig. 3. IRAS 100 μm map of the cirrus complex "BX" (adapted from Deul & Burton 1990) together with the positions of the absorption and emission measurements. The lowest contour is at 1.0 MJy $ster^{-1}$ and increases with steps of 0.3 MJy $ster^{-1}$

CH06– This field is 1°.6 (2.8 pc) from CH05n1 and contains three continuum sources revealing discrete absorption components near $v = 0$, and -15 km s^{-1}. The distance on the sky between these sources varies from 5 to 17 arcmin (0.1 to 0.5 pc). CH06n1 and CH06n2 are only 12 arcmin apart (0.3 pc), yet there are large differences between their spectra. Only the component near $v = -15$ km s^{-1} shows up in absorption in CH06n1, for which we derive a spin temperature of only 22 K. The narrow component seen in emission near $v = 0$ km s^{-1} has $T_{spin} > 200$ K; the broad component near -45 km s^{-1} has $T_{spin} > 25$ K. In CH06n2 the $v = 0$ km s^{-1} component has a spin temperature $T_{spin} = 480$ K; the $v = -15$ km s^{-1} feature

© European Southern Observatory • Provided by the NASA Astrophysics Data System

1994A&A...281..199S

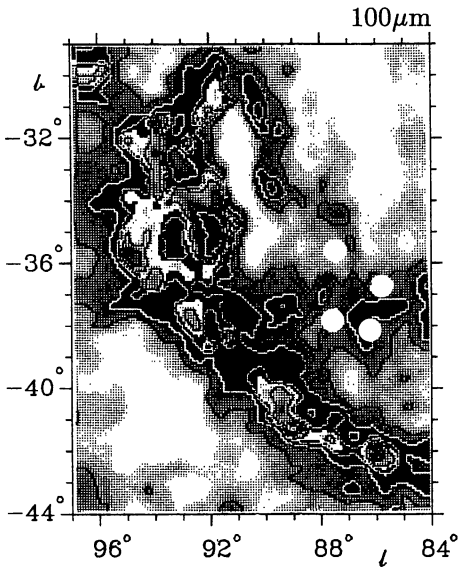

Fig. 4. IRAS 100 μm map of the cirrus cloud "CH" (adapted from Deul & Burton 1990) together with the positions of the absorption and emission measurements. The lowest contour is at 3.6 MJy ster^{-1} and increases with steps of 1.1 MJy ster^{-1}

is also seen in absorption, with $T_{\rm spin}$ = 180 K. The $v = -45$ km s^{-1} feature does not show up in absorption, giving the limit $T_{\rm spin} > 300$ K. CH06n3 is located 4 arcmin (0.1 pc) from n2 and 14 arcmin (0.4 pc) from n1; we derive $T_{\rm spin} > 60$ K as a weak lower limit to the spin temperature of the individual components.

4. Discussion

4.1. Spin temperatures

We find a large range of spin temperatures, characterizing the clumps of H I gas associated with dust cirrus. The derived spin temperatures are apparent ones, because we do not take into account mixing of gas at different temperatures in each velocity channel. These temperatures are therefore harmonic mean temperatures (van de Hulst et al. 1954), also known as "naively–derived spin tempertures" (Kulkarni & Heiles 1987). We also assume the H I emission to be distributed homogeneously over the entire 9 arcmin FWHM Effelsberg beam, so that the absorption in the small synthesized VLA beam (5 arcsec) corresponds to the column density. The derived apparent temperatures are therefore lower limits for the warm gas and upper limits for the cold component. A similar problem occurs when deriving dust temperatures from IRAS 60 μm /100 μm brightness ratios if two dust populations with different temperature distributions are present in these FIR bands (see e.g. Schwering 1988, or Draine 1990).

We can estimate the contribution of the warm gas to the emission spectra in those cases where we can isolate a discrete emission feature at the same velocity as the absorption feature; the contribution of this warm gas may then be eliminated via a baseline fit to the spectrum outside this distinct feature. This method was used first by Radhakrishnan et al. (1972), and later by Mebold et al. (1982). The spin temperatures we find in this way are somewhat lower than those found in Table 1. This is a very subjective procedure, because of the large solid-angle difference between the absorption and emission beams. It is clear however that most of the emission comes from warm gas. The clouds are a blend of cool ($\sim$ 100 K) and warm ($\sim$ 500 K) gas, not exclusively cool. The derived temperatures for the cool gas agree well with those of the diffuse clouds observed with the Copernicus satellite (e.g. van Dishoeck & Black 1986). Temperatures below 20 K in the diffuse medium are difficult to explain, since heating by metals only would already yield a temperature of 20 K (e.g. Field 1974). The derived temperature of 9 K toward BX07n3 is probably unreal and due to noise at the 3σ level in the absorption spectrum.

The spin temperatures we derive are somewhat higher than the temperatures of diffuse H I gas at lower latitudes derived by Kalberla et al. (1985). They find excitation temperatures between 34 and 74 K. The situation is different for cirrus structures at high galactic latitude, where we would in any case expect higher temperatures based on the fact that the lower density at high latitudes would, in the case of pressure equilibrium, have to be compensated for by a higher temperature. The question if such an equilibrium exists in cirrus structures is discusssed below.

4.2. A model for these cirrus clouds

The origin of the intermediate negative velocity (INV) H I gas ($v < -20$ km s^{-1}) remains an open problem. The velocities cannot be explained in terms of conventional galactic differential rotation, especially at high galactic latitudes where the disk H I would be restricted to nearby distances ($d \simeq 100$ pc) and hence to velocities $|v| = 0 \pm 7$ km s^{-1}. At low galactic latitudes the INV gas may be associated with the galactic warp. But at high $|b|$ it may be due to an interaction of high velocity (HVC) gas ($|v| > 70$ km s^{-1}) with gas of the galactic disk (e.g. Burton & Moore 1979). This high velocity gas could be: 1) infalling gas from the galactic halo or from extragalactic origin (Oort 1966, 1970); 2) hot gas raised by supernova explosions from the disk of our Galaxy, which cools by adiabatic expansion, and finally condenses into HVC's that fall back (Shapiro & Field 1976; Bregman 1980). The observational properties of HVC clouds were extensively studied by Wakker (1990).

The intermediate velocity gas appears to be local velocity gas which has been displaced to form intermediate velocity gas (Wesselius & Fejes 1973). Candidate drivers for such a disturbing event are (groups) of young stars, or supernovae (see overview by Heiles 1979). Despite the unresolved origin of the INV clouds, it is clear that they induce shocks when they move through the interstellar medium. We discuss our observations in the light of the models of Tenorio–Tagle et al. (1980, 1986, 1987), concerning the collision of clouds falling into the galactic disk.

Consider a cloud with density n_c, moving at high velocity v_c into the galactic disk. The density of the disk gas is n_g.

© European Southern Observatory • Provided by the NASA Astrophysics Data System

1994A&A...281..199S

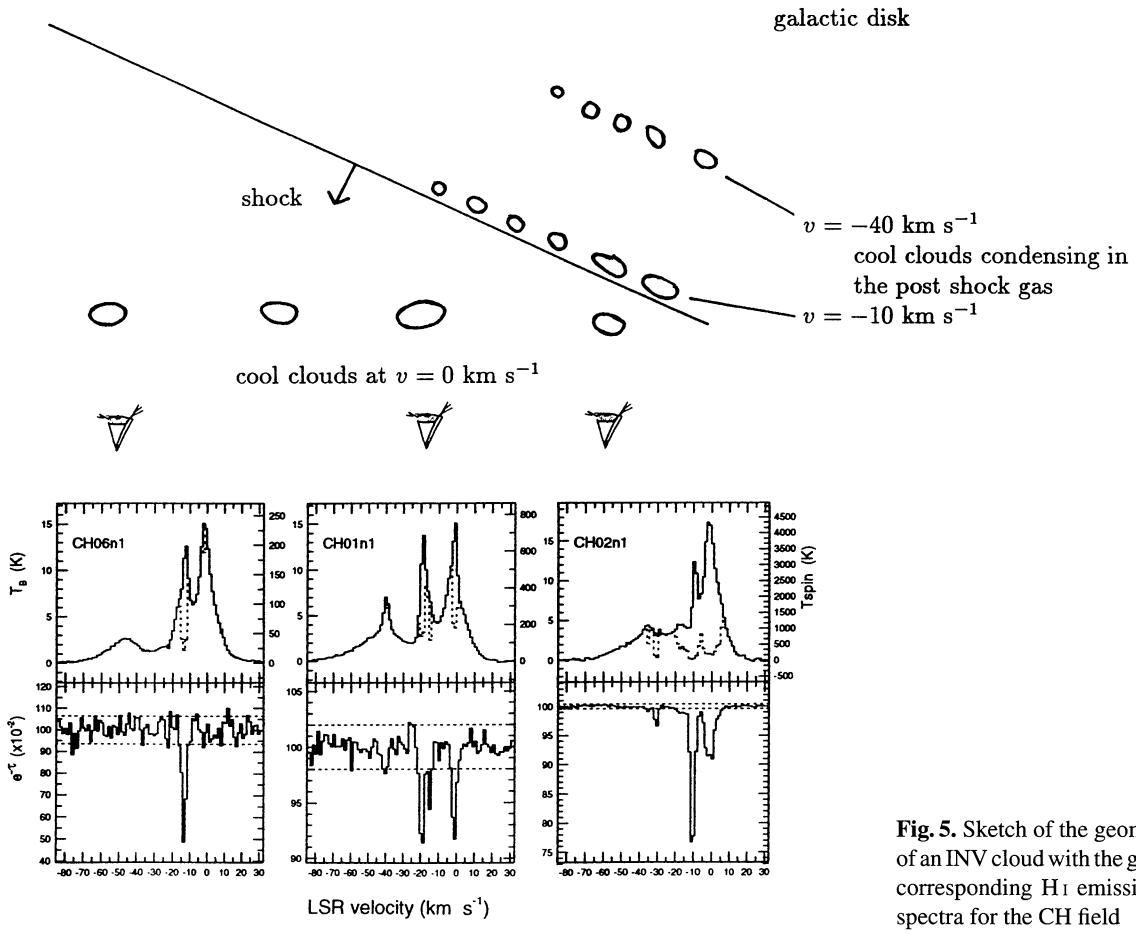

Fig. 5. Sketch of the geometry of a collision of an INV cloud with the galactic disk and the corresponding HI emission and absorption spectra for the CH field

Two shock fronts result from that collision, moving in opposite directions: one in the galactic disk, and one in the impinging cloud. They generate a layer of compressed gas in between them, which is pushed into the Galaxy at a velocity

$$v_l = v_c \frac{a}{1+a} \qquad (2)$$

where v_l is the velocity with respect to the reference system of the galactic disk gas which is assumed to be at rest, and $a = \sqrt{\frac{n_c}{n_g}}$. The collision ends when one of the shocks has passed through the whole galactic disk, or through the complete cloud. At the end of this collision, the velocity of the shocked layer remains supersonic in relation to the unperturbed galactic gas. After the shock has passed, the gas will cool by line radiation. When the temperature drops below 4000 K the cooling becomes very effective, since molecules like H_2 and CO may be (re-) formed in the recombination zone. In the CH field CO has been found (Magnani et al. 1985), Liszt & Burton (1979) report CO($J = 1 \rightarrow 0$) emission at $v = -9.4$ km s^{-1} toward 3C454.3. In the other fields CO has not yet been searched for, but we note that such a search would call for high spatial resolution, because of the clumpy cloud structures.

It is clearly seen from Eq.(2) that an HVC cloud with a velocity of 100 km s^{-1} causes an INV cloud with a velocity of 50 km s^{-1} when it collides with a galactic disk cloud of equal density. Meyerdierks (1991) uses this scenario to show that the observed high-, intermediate-, and low- velocity HI gas in the North Celestial Pole (NCP) Loop region are interrelated. He applies the collision theory of Tenorio–Tagle et al. to a two phase medium where cold disk clouds are immersed in a warm intercloud medium, and describes the collision of an HVC cloud in two steps: 1) an interaction of the HVC cloud with the intercloud medium, which leaves behind a moderately changed high velocity component because of the low density of the intercloud medium compared to the impinging cloud; 2) an interaction of this moderately changed HVC with a disk cloud of comparable density, causing the INV clouds. We searched through the list of HVC's of Wakker & van Woerden (1991), to see if there are HVC clouds on the sky in the direction of our cirrus clouds. We find two complexes: at $l = 263\overset{\circ}{.}5$, $b = 75\overset{\circ}{.}1$, $v = 100$ km s^{-1} and $l = 83\overset{\circ}{.}0$, $b = -36\overset{\circ}{.}0$, $v = -360$ km s^{-1} which are close to our BX and CH fields, respectively. The CH complex resembles the NCP Loop geometry described by Meyerdierks. The velocity sign of the HVC complex in the direction of the BX field suggests that it is most probably a line of sight superposition of an unrelated object. The missing HVC remnant in this case may have had a lower impinging velocity and/or has been dissolved through evolution. The scenario given above is consistent with

© European Southern Observatory • Provided by the NASA Astrophysics Data System

1994A&A...281..199S

the idea that the INV clouds are swept up regions behind shock fronts, as proposed by Siluk & Silk (1974), and is therefore also applicable to the displacement model.

There is substantial evidence for a shock interaction. The H I spectra (Fig 1.) show local as well as intermediate negative velocities in the direction of the cirrus clouds. Both velocity components are well correlated with different aspects of the FIR cirrus clouds, as shown by Deul and Burton. The emission and absorption spectra show line components at discrete velocities; between these velocities the emission is weak and no absorption at all is found (Fig. 1). We find that the cool H I is mainly at low velocities. Only in three cases do we detect the INV H I component in absorption, and this we explain below. The evolution of the shock phase is visible by the change in velocity of the original INV components and change in the spin temperature of components caused by the shock. If their temperatures drop below 200 K, they will show up in absorption. This is in fact what we see in the cirrus clouds AF, BX, and CH (Fig. 1). There is a change in the velocity of the broad INV component in the sequences: AF01n1, n2; and BX05n1, n3, n2, BX06n1, BX02n1, BX06n4, n2, n3, BX07; as well as in the sequence CH05n1, CH06n1, n3, n2, CH02n1, CH01n1. The INV moves to lower velocities and a narrow component shows up superimposed on it during its move, and it also turns up in absorption. Then the INV narrow component begins to weaken when the broad component vanishes in the low velocity gas. This is in agreement with the scenario of Tenorio–Tagle et al. (1987) who found from their models that all the collisional structures will eventually dissolve, given enough time. The low velocity cirrus clouds can easily be the older and decelerated version of the INV clouds. This could explain why cirrus clouds with local velocities appear generally to have a fossil shock morphology (Sect. 1). Figure 5 shows a sketch of the geometry of a collision of an INV cloud with the galactic disk for the CH field.

Because of the shocks, we cannot expect these cirrus clouds to be in a thermal steady state. A shock explains the large range in temperatures that we find: different parts of the cloud are at present at a different stage of shock completion. Shocks also cause dust processing. Evolution of dust grains, i.e. cycling of interstellar matter between the solid state and the gas state, has been suggested by Boulanger (1991) to explain the large IR colour variations observed on small scales in cirrus. Deul and Burton found large difference in 60 μm/100 μm colours between the normal and INV components in the cirrus studied in this paper. They found systematically higher 60 μm/100 μm brightness ratios for the INV gas. This effect can be caused by destruction in fast shocks ($v > 40$ km s^{-1}) of the largest grains ($a > 500$ Å, McKee et al. 1987; Seab 1987) responsible for the 100 μm emission. The absence of optical reflection of these cirrus on POSS plates supports such an explanation. Seab (1987) argues that small grains tend to survive radiative shocks, while they are destroyed in adiabatic shocks. This could also influence the 60 μm emission. Alternatively a higher 60/100 brightness ratio can be caused by a contribution of the O I line at 63 μm, which is one of the major energy escape channels in low density radiative shocks (Hollenbach et al. 1990). In addition, the oxygen abundance may be enhanced by dust processing in shocks, analogous to the Routley–Spitzer (1952) effect.

5. Conclusions

We determine the H I gas temperature in high galactic latitude cirrus structures from a combination of absorption and emission measurements. The temperatures we find range between 20 K and > 350 K. The low temperatures belong to the coldest clumps in the clouds. Cirrus have a filamentary structure, clearly visible at optical and IR wavelengths, with a low volume filling factor (0.2 according to Van Buren 1989). Therefore these clumps represent only the colder cores of much more widely distributed and warmer H I gas. Probably most of the space in the cirrus clouds is filled with warm ($T > 200$ K) H I gas that absorbs imperceptibly. A better way to determine the emission associated with the absorption clumps, would involve comparison of synthesis absorption and emission observations combined with zero-spacing information (see Kalberla et al. 1985), where one could possibly identify and separate in emission the same clumps we see in absorption. We plan to undertake such a study in the near future.

The large variation in observed temperatures on scales as small as 9 arcmin (which corresponds to 0.3 pc at the adopted distance of 100 pc) within the individual clouds is explained by a collision with galactic disk clouds. This model is suggested by the intermediate–velocity components which are present in the H I emission spectra, as well as by the absence of absorption and emission at velocities between the intermediate– and local–velocity components. In a few cases we find absorption in the INV components. We argue that different parts of the clouds are at present in different shock phases. The INV components will only show up in the post-shock gas when the H I gas temperature has dropped below 200 K. In this context all cirrus clouds with a fossil shock morphology are the ultimate fate of the INV clouds.

The IRAS 60 μm/100 μm brightness ratio in the components of a cirrus cloud characterized by an anomalous velocity is significantly higher than in the components at low velocities (Deul & Burton 1990). This suggests shock processing of the dust and/or the gas in these clouds. The ISO satellite will be a powerful tool for investigating the nature of these high 60 μm/100 μm brightness ratios.

Acknowledgements. The VLA is operated by the National Radio Astronomy Observatory, under contract with the National Science Foundation. The Effelsberg telescope is operated by the Max–Planck–Institut für Radioastronomie in Bonn. Visits by John Dickey to the Leiden Observatory were supported by a visitor's grant from the Nederlandse Organisatie voor Wetenschappelijk Onderzoek (NWO). The visit of Ronald Stark to the University of Minnesota was supported by NWO and by the Leids Kerkhoven Bosscha Fonds. He also wishes to thank the Astronomy Department of the University of Minnesota for its hospitality.

© European Southern Observatory • Provided by the NASA Astrophysics Data System

1994A&A...281..199S

References

Boulanger F. 1991 in E. Falgarone, F. Boulanger, G. Duvert (eds.) Fragmentation of Molecular Clouds and Star Formation, IAU 147. Kluwer, Dordrecht, p. 151

Boulanger F., Baud B., van Albada G.D. 1985 A&A 144, L9

Bregman J. 1980 ApJ 236, 577

Bridle A.H., Davis M.M., Fomalont E.B., Lequeux J. 1972 AJ 77, 405

Burton W.B., Bania T.M., Hartmann, D., Yuan T. 1992 in J. Palouš, W.B. Burton, P.O. Lindblad (eds.) Evolution of Interstellar Matter and Dynamics of Galaxies. Cambridge Univ. Press, p. 25

Burton W.B., Moore R.L. 1979 AJ 84, 189

Condon J.J., Broderick J.J. 1985 AJ 90, 2540

Condon J.J., Broderick J.J. 1986 AJ 91, 1051

Deul E.R. 1988 PhD Thesis University of Leiden

Deul E.R., Burton W.B. 1990 A&A 230, 153

Dickey J.M., Salpeter E.E., Terzian Y. 1978 ApJS 36, 77

Dickey J.M., Brinks E., Puche D. 1992 ApJ 385, 501

van Dishoeck E.F., Black J.H. 1986 ApJS 62, 109

Draine B.T. 1990 in H.A. Thronson and J.M. Shull (eds.) The Interstellar Medium in Galaxies. Kluwer, Dordrecht, p. 483.

Field G.B. 1974 in R. Balian, P. Encrenaz, J. Lequeux (eds.) Atomic and Molecular Physics and the Interstellar Matter. North–Holland, Amsterdam, p. 469

Goldsmith D.W., Habing H.J., Field G.B. 1969 ApJ 158, 173

Gredel R., van Dishoeck E.F., de Vries C.P., Black J.H. 1992 A&A 257, 245

Harwit M., Houck J.R., Stacey G.J. 1986 Nature 319, 646

Heiles C. 1979 ApJ 229, 533

Heiles C., Habing H.J. 1974 A&AS 14, 1

Hollenbach D.J., Chernoff D.F., McKee C.F. 1990 in B.H. Kaldeich (ed.) Infrared Spectroscopy in Astronomy ESA SP–290. ESA Publications Division, ESTEC, Noordwijk, p. 245

van de Hulst H.C. 1957 in H.C. van de Hulst (ed.) Radioastronomy, IAU 4. Cambridge University Press, p. 3

van de Hulst H.C., Muller C.A., Oort J.H. 1954 BAN 12, 116

Kalberla P.M.W., Mebold U., Reich W. 1980 A&A 82, 275

Kalberla P.M.W., Mebold U., Reif K. 1982 A&A 106, 190

Kalberla P.M.W., Schwartz U.J., Goss M.W. 1985 A&A 144, 27

Kulkarni S.R., Heiles C. 1987 in D.J. Hollenbach and H.A. Thronson (eds.) Interstellar Processes. Reidel, Dordrecht p. 87

Liszt H.S., Burton W.B. 1979 ApJ 228, 105

Low F.J., Beintema, D.A., Gautier T.N. et al. 1984 ApJ 278, L19

Magnani L., Blitz L., Mundy L. 1985 ApJ 295, 402

McKee C.F., Hollenbach D.J., Seab C.G., Tielens A.G.G.M. 1987 ApJ 318, 674

Mebold U., Winnberg A., Kalberla P.M.W., Goss W.M. 1982 A&A 115, 223

Meyerdierks H. 1991 A&A 251, 269

Oort J.H. 1966 BAN 18, 421

Oort J.H. 1970 A&A 7, 381

Penprase B.E. 1992 ApJS 83, 273

Radhakrishnan V., Murray J.D., Lockhart P., Whittle R.P.J. 1972 ApJS 24, 15

Routley P. McR., Spitzer L. Jr. 1952 ApJ 115, 227

Schwering P.B.W. 1988 PhD Thesis University of Leiden

Seab C.G. 1987 in D.J. Hollenbach and H.A. Thronson (eds.) Interstellar Processes. Reidel, Dordrecht, p. 491

Shapiro P.R., Field G.B. 1976 ApJ 295, 762

Siluk R.S., Silk J. 1974 ApJ 192, 51

Stark R. 1990 A&A 230, L25

Stark R. 1993 in preparation

Tenorio–Tagle G. 1980 A&A 88, 61

Tenorio–Tagle G., Bodenheimer P., Różyczka M., Franco J. 1986 A&A 170, 107

Tenorio–Tagle G., Franco J., Bodenheimer P., Rozyczka M. 1987 A&A 179, 219

Van Buren D. 1989 ApJ 338, 147

Wakker B.P. 1990 PhD Thesis University of Groningen

Wakker B.P., van Woerden H. 1991 A&A 250, 509

Wesselius P.R., Fejes I. 1973 A&A 24, 15

This article was processed by the author using Springer-Verlag TEX A&A macro package 1992.

© European Southern Observatory • Provided by the NASA Astrophysics Data System